PNAS
Proceedings of the National Academy of Sciences of the United States of America www.pnas.org

The Isolation by Crystallization of Translational Isomers of a Bistable Donor-Acceptor [2]Catenane

*Cheng Wang[†±], Mark A. Olson[†±], Lei Fang[†], Diego Benítez[ϕ], Ekaterina Tkatchouk[ϕ], Subhadeep Basu[†], Ashish N. Basuray[†], Deqing Zhang[‡], Daoben Zhu[‡], William A. Goddard [ϕ], and J. Fraser Stoddart[†]**

[†] Department of Chemistry, Northwestern University, Evanston, Illinois 60208, USA

[‡] Beijing National Laboratory for Molecular Sciences, Organic Solids Laboratory, Institute Of Chemistry, Chinese Academy of Sciences, Beijing 100080, China

[ϕ] Materials and Process Simulation Center, California Institute of Technology, Pasadena, California 91125, USA

± These authors contributed equally to this work.

* To whom correspondence should be addressed.

Supplementary Information

1. General Method

All reagents and starting materials were purchased from Aldrich or VWR and used without further purification. 4,4′,(5′)-Bis(2-cyanoethylthio)tetrathiafulvalene (1, 2) (**3**), cyclobis(paraquat-*p*-phenylene) tetrakis(hexafluorophosphate) (3) (CBPQT·4PF_6), 1,1′-[1,4-phenylenebis(methylene)]-bis(4,4′-bipyridinium) bis(hexafluorophospate) (4), 1,5-bis[2-(2-(2-(2-hydroxyethoxy)ethoxy)ethoxy)ethoxy]naphthalene (5) (BHEEEEN) and 1,5-bis[2-[2-[2-(2-hydroxyethoxy)ethoxy]ethoxy]ethoxy]naphthalene bis(4-methyl-benzenesulfonate) (5) were prepared following procedures recorded in the literature. All reactions were performed under an argon atmosphere and in dry solvents unless otherwise noted. Analytical thin-layer chromatography (TLC) was performed on aluminum sheets, precoated with silica gel 60-F_{254} (Merck 5554). Column chromatography was carried out using silica gel 60 (Silicycle) as the stationary phase. Deuterated solvents (Cambridge Isotope Laboratories) for NMR spectroscopic analyses were used as received. NMR spectra were recorded on Bruker Avance-500 at 500 MHz and Bruker Avance-600 at 600 MHz spectrometers at ambient temperature. All chemical shifts are quoted in ppm relative to the signals corresponding to the residual non-deuterated solvents ($CDCl_3$: 7.26 ppm, CD_3CN: 1.94 ppm). High resolution electrospray ionization (HR ESI) mass spectra were measured on Agilent 6210 LC-TOF with Agilent 1200 HPLC introduction. High-resolution matrix-assisted laser desorption/ionization (MALDI) mass spectra were measured on a Bruker Autoflex III mass spectrometer. UV-Vis spectra were recorded on a Varian 100-Bio UV/Vis spectrophotometer. The purity of the [2]catenane **1**·4PF_6 was characterized by analytical HPLC. It was performed on an Analytical RP-HPLC instrument, using a C_{18} column. Isothermal Titration

Microcalorimetry was carried out using a Microcal VP-ITC titration microcalorimeter. Software provided by Microcal LLC was used to compute the thermodynamic parameters of the titration ($\Delta G°$, K_a, $\Delta S°$, $\Delta H°$) based on the one-site binding model. Aliquots (5–10 μL) of degassed solutions of the guest in MeCN were titrated with stirring into solutions of the host at 298 K. The heat of dilution for each titration was measured by determining the heat released on the injection of the guest into MeCN in the absence of host, and the enthalpy of dilution was subtracted from the enthalpy of the titration to determine the enthalpy of complexation. Electrochemical experiments were carried out at room temperature in argon-purged aqueous solutions, with a Gamry Reference 600 potentiostat interfaced to a PC. Cyclic voltammetry experiments were performed using a glassy carbon working electrode (0.018 cm^2, Cypress Systems). Its surface was polished routinely with 0.05 μm alumina-water slurry on a felt surface immediately before use. The counter electrode was a Pt coil and the reference electrode was a standard Ag/AgCl electrode. The concentration of the sample and supporting electrolyte (lithium perchlorate) were 5×10^{-4} mol/L and 0.1 mol/L, respectively. Powder X-ray diffraction studies were conducted using a calibrated Rigaku-D/MAX-A X-Ray diffractometer with Bragg–Brentano parafocusing geometry, with a conventional copper target X-ray tube set to 40 KV and 20 mA. Data was acquired using a ½ divergence and scatter slits, 0.1 receiving slit, at 0.05 step with a 5 sec/point scan rate. The X-ray crystal data for translational isomers **1R**·$4PF_6$ and **1G**·$4PF_6$ were collected at 173 K using a Rigaku 007HF RA generator (Mo-K_α radiation) equipped with confocal optics and Saturn 944+ CCD system. Intensities were corrected for Lorentz-polarization and for absorption. The structures were solved by direct methods. Hydrogen atoms bound to carbon were idealized.

Structural refinements were obtained with full-matrix least-squares based on F^2 by using the program SHELXTL. CCDC 782651 and CCDC 782652 contain the supplementary crystallographic data for this paper. These data (excluding structural factors) can be obtained free of charge via www.ccdc.ac.uk/conts/retrieving.html or from the Cambridge Crystallographic Data centre, 12 Union Road, Cambridge CB2 1EZ, UK; fax (+44) 1223-336-033; e-mail: deposit@ccdc.cam.ac.uk.

2. Chemical Synthesis

Scheme S1. Synthesis of compound **2**

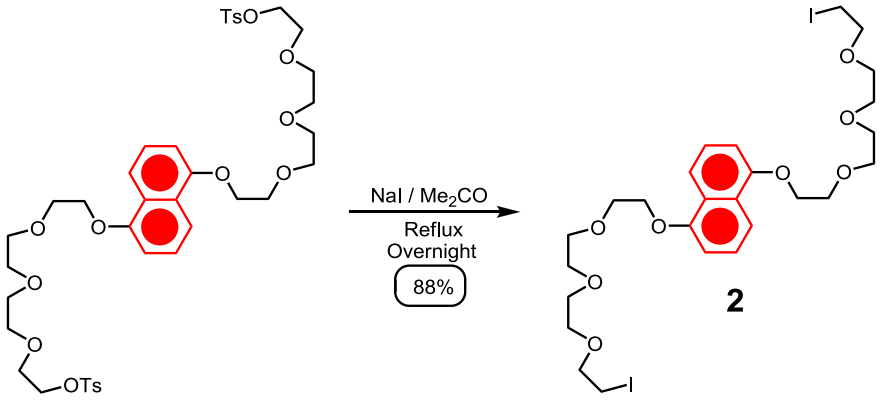

2: 1,5-Bis[2-[2-[2-(2-hydroxyethoxy)ethoxy]ethoxy]ethoxy]naphthalene bis(4-methyl-benzenesulfonate) (1.31 g, 1.58 mmol) and sodium iodine (2.37 g, 15.8 mmol) were dissolved in dry Me_2CO (100 mL), and the reaction mixtureb was heated under reflux overnight. After cooling down to the room temperature, CH_2Cl_2 (200 mL) was added to the reaction mixture and the organic phase was washed with H_2O (3 × 100 mL). The organic layer was then dried (Na_2SO_4), filtered and the solvent evaporated under reduced

pressure to afford the crude compound **2** as a yellow oil (1.03 g, 88%). The crude product was used directly for the next step.

Scheme S2. Synthesis of macrocycle **4** and the bistable [2]catenane **1**·4PF_6

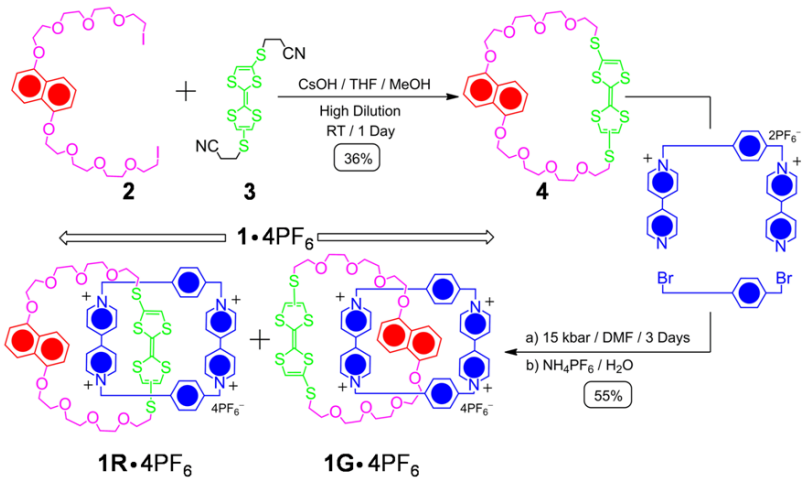

4: A solution of **2** (0.74 g, 1.0 mmol) and **3** (0.37 g, 1.0 mmol) in anhydrous degassed THF (50 mL) was added very slowly to a solution of CsOH·H_2O (0.40 g, 2.29 mmol) in anhydrous degassed THF (100 mL) and MeOH (20 mL) during 20 h. The reaction was stirred for a further 4 h. The solvents were evaporated under reduced pressure and the resulting residue was purified by column chromatography [SiO_2 : EtOAc / CH_2Cl_2 (1 : 3)]. The product **4** was isolated as a yellow oil (0.27 g, yield, 36%). ^{1}H NMR ($CDCl_3$, 500 MHz, 298 K, ppm): δ = 2.83 (t, *J* = 6.5 Hz, 4H), 3.82–3.57 (m, 20H), 4.01 (t, *J* = 4.5 Hz, 4H), 4.32 (t, *J* = 4.5 Hz, 4H), 6.29 (s, 1.7H), 6.35 (s, 0.3H), 6.86 (d, *J* = 8.0 Hz, 2H), 7.35 (t, *J* = 8.0 Hz, 2H), 7.87 (d, *J* = 8.0 Hz, 2H). ^{13}C NMR ($CDCl_3$, 125 MHz, 298K, ppm): δ = 35.6, 68.3, 69.7, 69.8, 70.1, 70.9, 71.0, 71.1, 71.15, 71.17, 71.6, 106.1, 112.4, 115.0, 123.3, 123.6, 125.5, 126.5, 126.8, 127.1, 127.1, 154.7. MALDI–TOF MS: calcd for $C_{32}H_{40}O_8S_6$ *m/z* = 744.104 $[M]^+$, found: *m/z* = 743.844 $[M]^+$.

1·4PF_6**:** A mixture of 4,4′-bis(bromomethyl)benzene (105 mg, 0.40 mmol), the macrocycle **4** (100 mg, 0.13 mmol), and 1,1′-[1,4-phenylenebis(methylene)]-bis(4,4′-bipyridinium) bis(hexafluoro phospate) (55) (285 mg, 0.40 mmol) was dissolved in DMF (10 mL). The reaction mixture was subjected to 15 kbar in an ultra high pressure reaction chamber at room temperature for 3 d, the resulting green solution was subjected to column chromatography [SiO_2: Me_2CO / NH_4PF_6 (100 : 1, v / w)]. The green band was collected and most of the solvent was removed under reduced pressure, followed by the addition of H_2O (10 mL). The precipitate was collected by filtration and washed with H_2O (3 × 20 mL), to give an equimolar mixture of **1R**·4PF_6 and **1G**·4PF_6 as a green solid (132 mg, 55 %). ^{1}H NMR (CD_3CN, 600 MHz, 233K, ppm): δ = 2.29 (d, *J* = 8.0 Hz, ~1H), 2. 76–2. 82 (m, ~2H), 2.91–3.00 (m, ~2H), 3.40–4.30 (m, 28H), 5.54–5.94 (m, 10H), 6.17 (t, *J* = 7.9 Hz, ~1H), 6.20–6.25 (m, 1H), 6.43 (d, *J* = 7.6 Hz, ~0.95H), 6.54 (d, *J* = 7.7 Hz, ~0.05H), 7.14–8.09 (m, 18H), 8.58–9.01 (m, 8H). HR MS (ESI): Calcd for $C_{68}H_{72}F_{24}N_4O_8P_4S_6$ *m*/*z* = 1699.2594 $[M - PF_6]^+$, 777.1474 $[M - 2PF_6]^{2+}$, found *m*/*z* = 1699.2559 $[M - PF_6]^+$, 777.1475 $[M - 2PF_6]^{2+}$.

Scheme S3. Synthesis of compound **5**

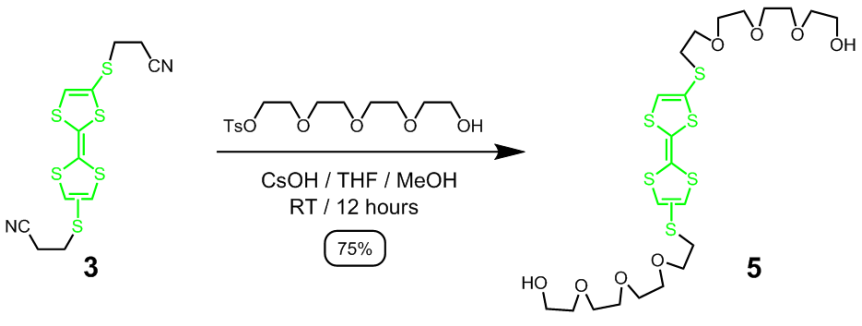

5: A solution of $CsOH \cdot H_2O$ (0.40 g, 2.29 mmol) in anhydrous degassed MeOH (5 mL) was added to a solution of **3** (0.37 g, 1.0 mmol) in anhydrous degassed THF (80 mL) over a period of 30 min.. The mixture was stirred for an additional 30 min. before a solution of tetraethyleneglycol monotoluenesulfonate (0.65 g, 2.15 mmol) in anhydrous degassed THF (20 mL) was added. The reaction mixture was stirred for 12 h. After removing the solvents under reduced pressure, the resulting mixture was purified by column chromatography [SiO_2 : EtOAc / CH_2Cl_2 / MeOH (8 : 8 : 1)]. The product **5** was isolated as red yellow oil (0.46 g, yield, 75%). ^{1}H NMR ($CDCl_3$, 500 MHz, 298K, ppm): δ = 2.91 (m, 4H), 3.71–3.56 (m, 28H), 6.40 (s, 2H). ^{13}C NMR ($CDCl_3$, 125 MHz, 298K, ppm): δ = 35.08, 35.10, 61.7, 69.7, 70.4, 70.5, 70.5, 70.7, 72. 6, 112.2, 112.3, 123.1, 123.2, 126.4, 126.5. MALDI–TOF MS: calcd for $C_{22}H_{36}O_8S_6$ *m/z* = 620.073 $[M]^+$, found: *m/z* = 620.094 $[M]^+$.

3. Analytical HPLC

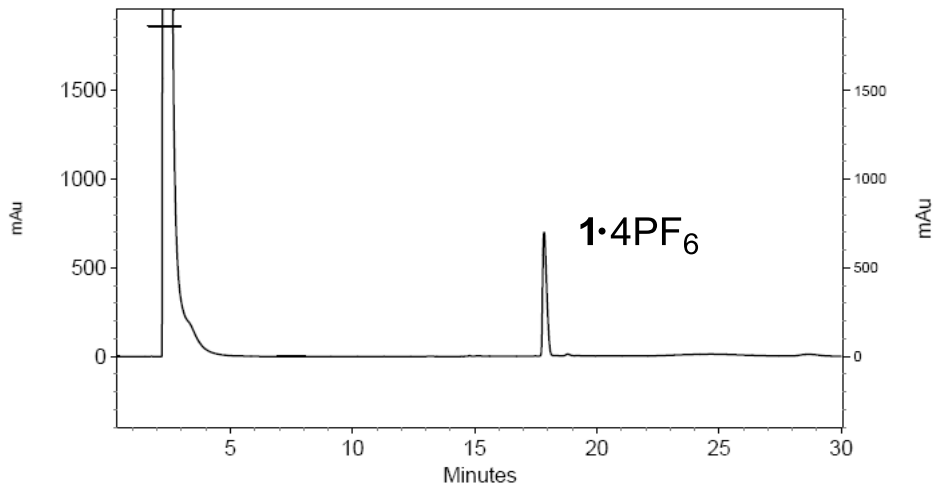

Fig. S1. The analytical RP-HPLC chromatogram of **1**·$4PF_6$ (water-MeCN 0-60% in 20 min, λ = 254 nm)

4. Isothermal Titration Microcalorimetry

Isothermal titration microcalorimetry (ITC) binding isotherms for $CBPQT^{4+}$ with compound **5** (STTFS-TEG) and BHEEEEN (DNP-TEG) were recorded in MeCN at 298 K (Scheme S4, Fig. S2). The reported values in Table S1 are the mean results of multiple titrations, and errors are reported as a standard deviation from the mean. The results showed that in MeCN, the binding of $CBPQT^{4+}$ with DNP-TEG is stronger than $CBPQT^{4+}$ with STTFS-TEG. Fig. S3 illustrates the comparison of potential-energy surfaces for the formation of two independent host-guest pseudorotaxanes (STTFS-TEG $\subset$ $CBPQT^{4+}$ and DNP-TEG $\subset$ $CBPQT^{4+}$) in MeCN.

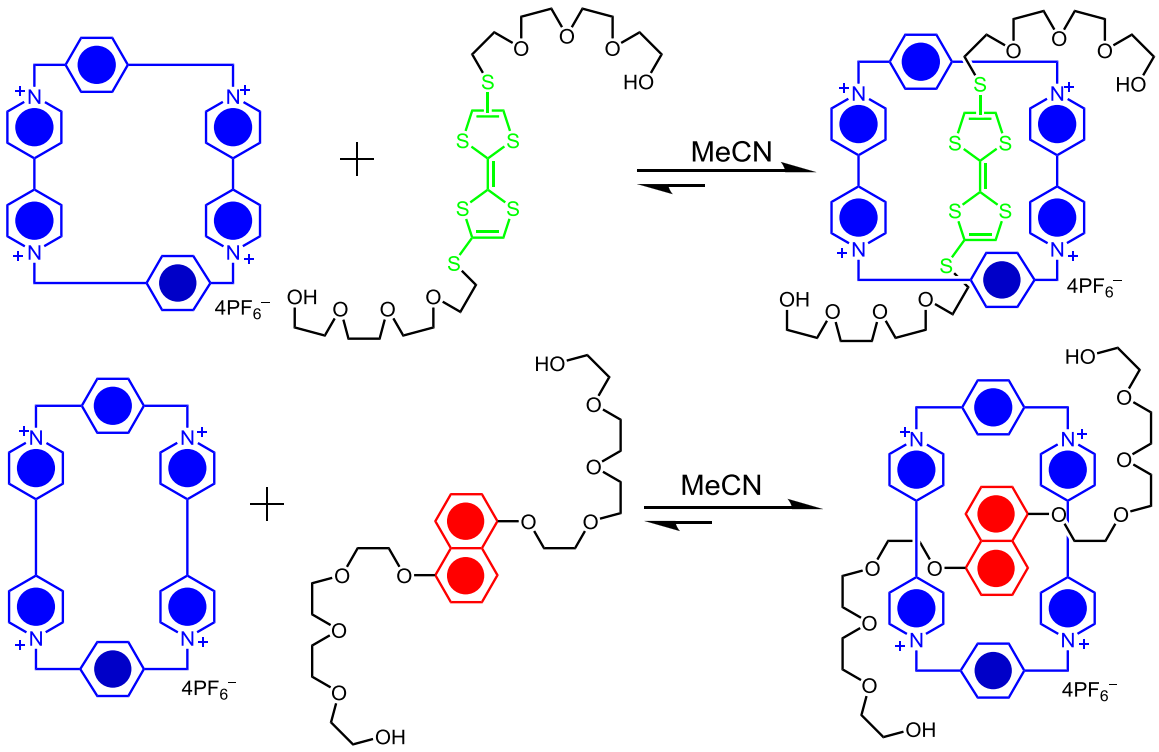

Scheme S4. The schematic representation illustrating the formation of the [2]pseudorotaxanes (STTFS-TEG $\subset$ $CBPQT^{4+}$ and DNP-TEG $\subset$ $CBPQT^{4+}$) in MeCN.

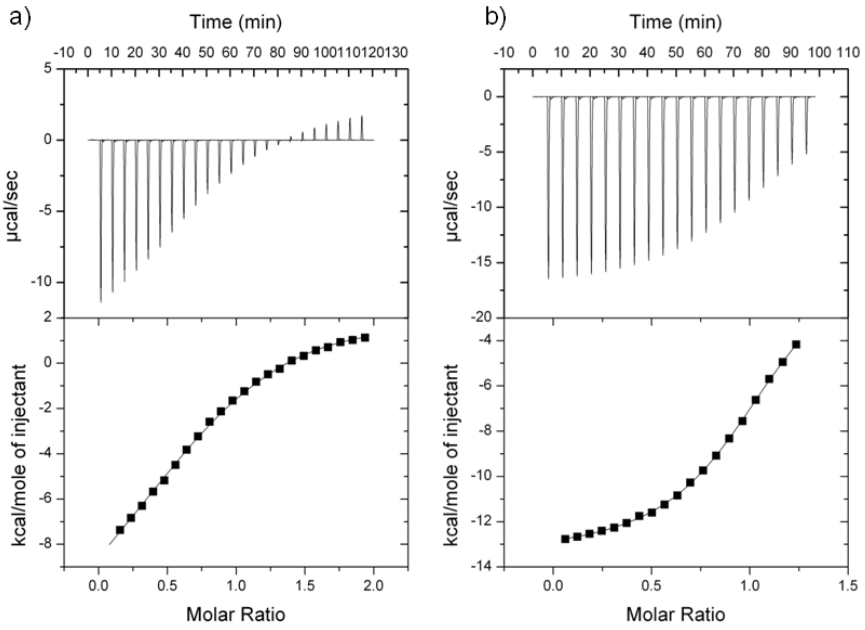

Fig. S2. Isothermal titration microcalorimetry binding isotherms for $CBPQT^{4+}$ with a) STTFS-TEG and b) DNP-TEG in MeCN at 298 K.

Table S1. Thermodynamic binding data[a] corresponding to the complexation between host $CBPQT^{4+}$ and STTFS-TEG and DNP-TEG guests in MeCN determined by Isothermal Titration Microcalorimetry at 298 K.

Guest	Solvent	ΔH^{o} [kcal·mol^{-1}]	ΔS^{o} [cal·mol^{-1}·K^{-1}]	$\Delta G^{o}_{298\ K}$ [kcal·mol^{-1}]	K_a [10^3 M^{-1}]
STTFS-TEG	MeCN	–10.60 (±0.76)	–17.6 (±2.5)	–5.36 (±0.14)	8.58 (±2.03)
DNP-TEG	MeCN	–13.62 (±0.13)	–24.4 (±0.4)	–6.34 (±0.03)	43.47 (±1.67)

[a] A 0.39 mM standard solution for $CBPQT^{4+}$ was used for all titrations into which solutions of various guests were added in 10 µL aliquots (3.9 mM STTFS-TEG; 3.9 mM DNP-TEG). Fits were performed using Microcal LLC software. The stoichiometry of all complexes was between 0.99 and 1.07 indicating a 1:1 complex is formed.

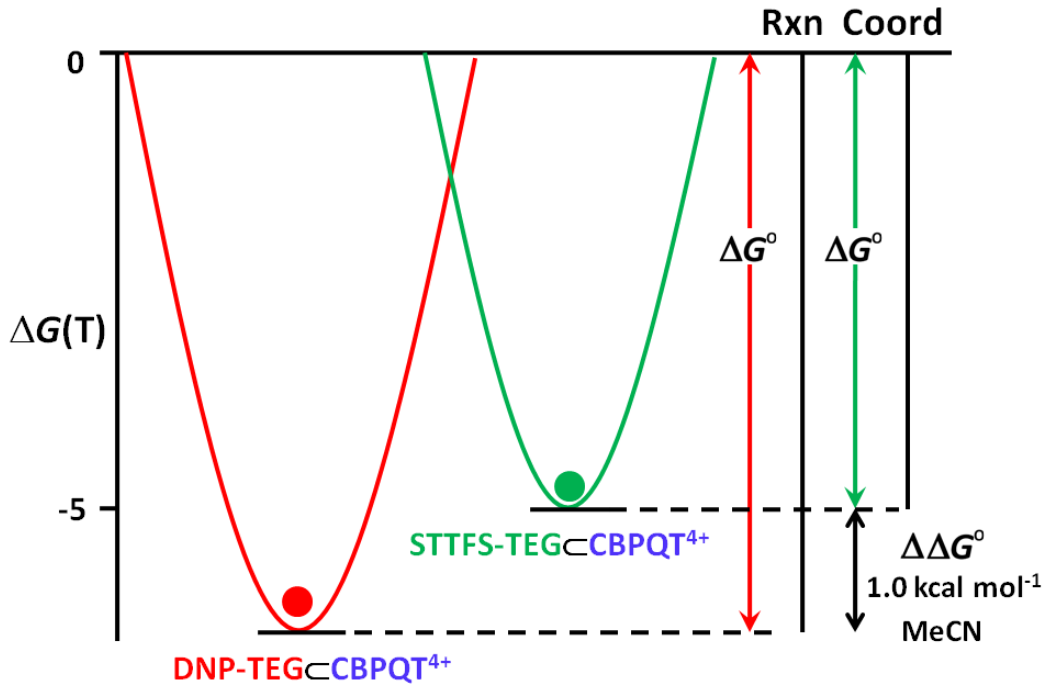

Fig. S3. A comparison of the two potential-energy surfaces for the formation of two independent host-guest pseudorotaxanes illustrating the decrease in free-energy of binding (ΔG^{o}) for DNP-TEG ⊂ $CBPQT^{4+}$ (red circle) and STTFS-TEG ⊂ $CBPQT^{4+}$ (green circle) in pure MeCN, and is defined against a normal reaction coordinate corresponding to the threading event.

5. ^{1}H NMR Spectroscopic Characterization

Since the ^{1}H NMR spectrum of **1**·4PF_6 in CD_3CN at room temperature reveals broad peaks because of the dynamic nature of the mechanically interlocked components, we recorded a ^{1}H NMR spectrum (Fig. S4a) of **1**·4PF_6 in CD_3CN at 233 K. All the peaks in this spectrum have been assigned based on ^{1}H-^{1}H gradient selected Double-Quantum-Filtered Correlation Spectroscopy (^{1}H-^{1}H-g-DQF-COSY) and the COSY spectrum (Fig. S4b) of **1**·4PF_6 in CD_3CN recorded at 233 K. According to the NMR spectra, two translational isomers of **1**·4PF_6 can be identified (Fig. S4a) in CD_3CN at 233 K. Based on

the integrals for the relevant proton resonances, e.g., the proton $H_{2/6}$, the ratio of translation isomers **1R**·$4PF_6$ and **1G**·$4PF_6$ were approximately 1:1 in CD_3CN at 233 K (Fig. S5a). It should be mentioned here that there are two configurational isomers for each translational isomer because of the cis-trans isomerization of the STTFS unit. According to the COSY spectrum, in CD_3CN, all the naphthalene protons ($H_{2/6}$, $H_{3/7}$ and $H_{4/8}$) in **1R**·$4PF_6$ show two sets of separated signals. For example, proton $H_{2/6}$ resonate at δ = 6.43 and 6.54 ppm. According to their corresponding integrals, the ratios of these two configurational isomers were calculated to be 1:20.

The ^1H NMR spectrum and the COSY spectrum of **1**·$4PF_6$ in CD_3COCD_3 were also recorded (Fig. S5) at 220 K. Based on the integrals for the particular resonances of the DNP proton, the ratios of translation isomers **1R**·$4PF_6$ and **1G**·$4PF_6$ was around 1:1.5 in CD_3COCD_3 at 220 K. However, each naphthalene proton ($H_{2/6}$, $H_{3/7}$ or $H_{4/8}$) in **1R**·$4PF_6$ show only one NMR signal, so that the cis-trans isomerization of STTFS cannot be observed in CD_3COCD_3 at this temperature.

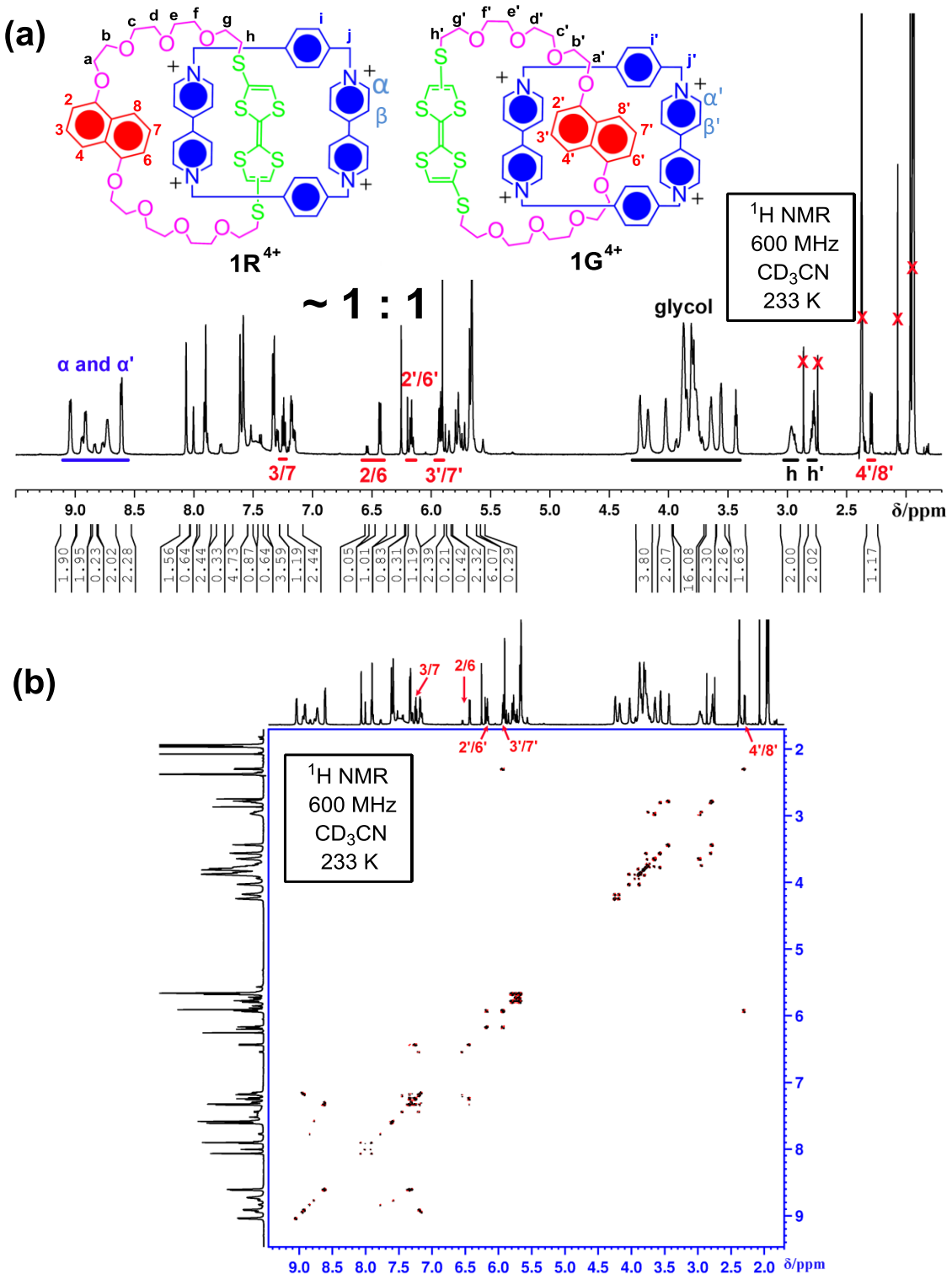

Fig. S4. ^{1}H NMR spectrum (a) and ^{1}H-^{1}H-g-DQF-COSY spectrum (b) of **1**·4PF_6 recorded in CD_3CN at 233 K. The ratio of translation isomers **1R**·4PF_6 and **1G**·4PF_6 is about 1:1.

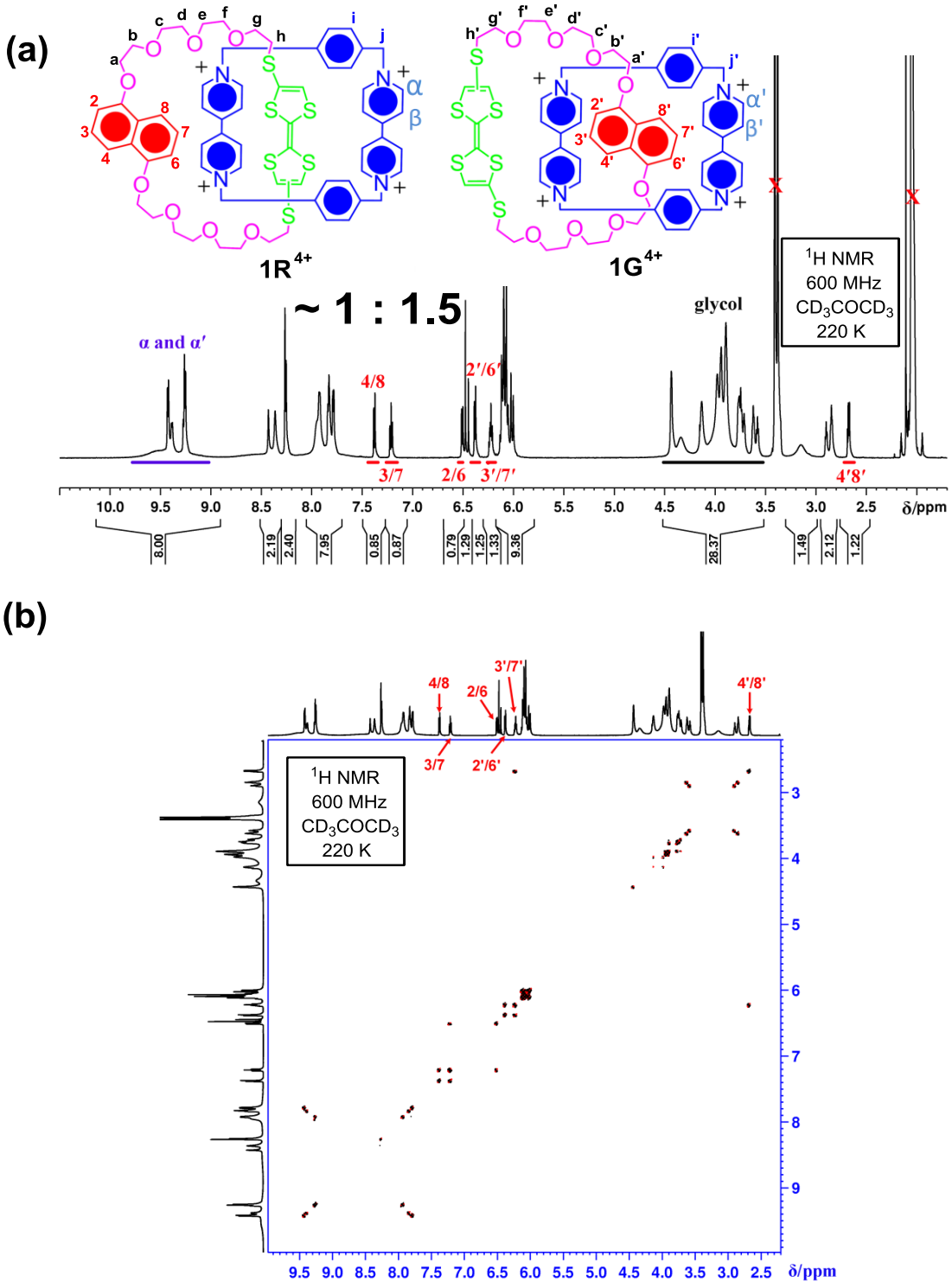

Fig. S5. ^{1}H NMR spectrum (a) and ^{1}H-^{1}H-g-DQF-COSY spectrum (b) of **1**·4PF_6 recorded in CD_3COCD_3 at 220 K. The ratio of translation isomers **1R**·4PF_6 and **1G**·4PF_6 is about 1:1.5.

6. UV/Vis Absorption Spectroscopic Characterization

Fig. S6 shows the UV/Vis absorption spectrum of **1**·4PF_6 recorded in MeCN at 298 K. The charge transfer (CT) absorption band centered on 800 nm is characteristic of structures in which a TTF unit is located inside the $CBPQT^{4+}$ ring. The CT band centered on 540 nm in the 500 ~ 560 nm region corresponds to the translational isomer when the DNP unit is located inside the $CBPQT^{4+}$ ring.

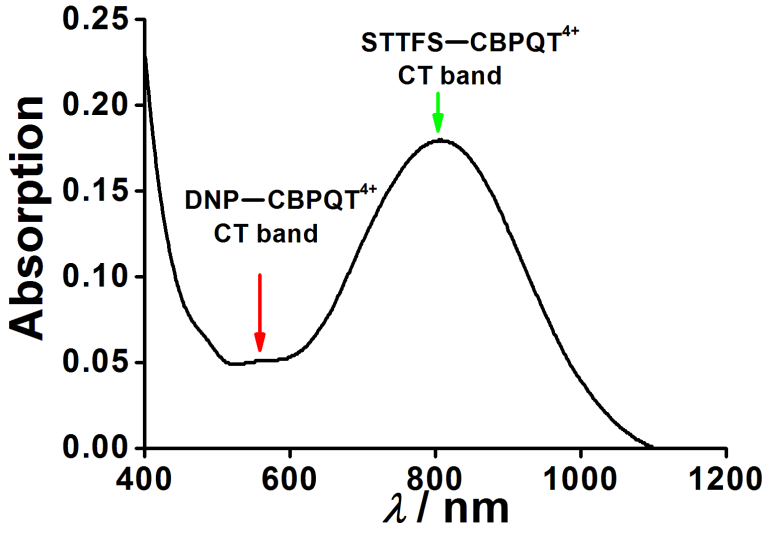

Fig. S6. The UV spectra of **1**·4PF_6 (1.0×10^{-4} M) recorded in MeCN at 298 K

6. Electrochemical Behavior

The cyclic voltammetry (CV) traces of the model compound STTFS-TEG and **1**·4PF_6 in MeCN at 298 K are shown in Fig. S7. In MeCN, the bare STTFS-TEG has two reversible redox potentials at +418 mV and +673 mV (*vs* Ag/AgCl), corresponding to the reversible two electron oxidation of STTFS (STTFS→$STTFS^{+\cdot}$ and $STTFS^{+\cdot}$→ $STTFS^{2+}$) to the radical dication. By contrast, we observed two oxidization potentials at +415 and +646

mV for **1**·4PF_6 in MeCN. The oxidation potential at +415 mV arises from the STTFS→$STTFS^{+\cdot}$ process when the STTFS unit resides on the outside of the $CBPQT^{4+}$ ring. The oxidation potential at +646 mV arises from the $STTFS^{+\cdot}$→ $STTFS^{2+}$ process for both the translational isomers of **1**·4PF_6. These CV results are consistent with the existence of two translational isomers of **1**·4PF_6 as indicated already by ^{1}H NMR spectroscopy (Fig. S4) in CD_3CN and UV/Vis spectroscopy (Fig. S6).

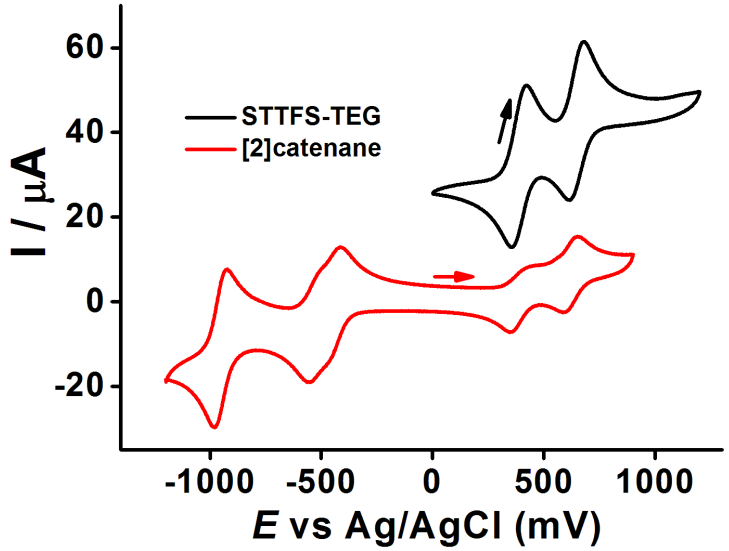

Fig. S7. The cyclic voltammograms spectra of **1**·4PF_6 and STTFS-TEG recorded in MeCN at 298 K.

By varying CV scans rates, various kinetic parameters for relaxation from the translational **1G**·4PF_6 to the translational **1R**·4PF_6 have been investigated in MeCN. Fig. S8 shows the series of second scan CVs of **1**·4PF_6 in MeCN. We have taken into account the rates based on the integrated current at +415 mV relative to the total current of the first-oxidation peaks of both translational isomers. However, a first order decay model could not be fitted to the population ratios of the translational isomers and the relaxation

times because the relaxation process is too fast to be detected by CV experiments at 298 K in MeCN. That means the τ value is on the order of 0.1 s < τ < 0.5 s. And the analysis of the CV reveals a ratio for **1G**·4PF_6 : **1R**·4PF_6 of 53:47 in MeCN at room temperature.

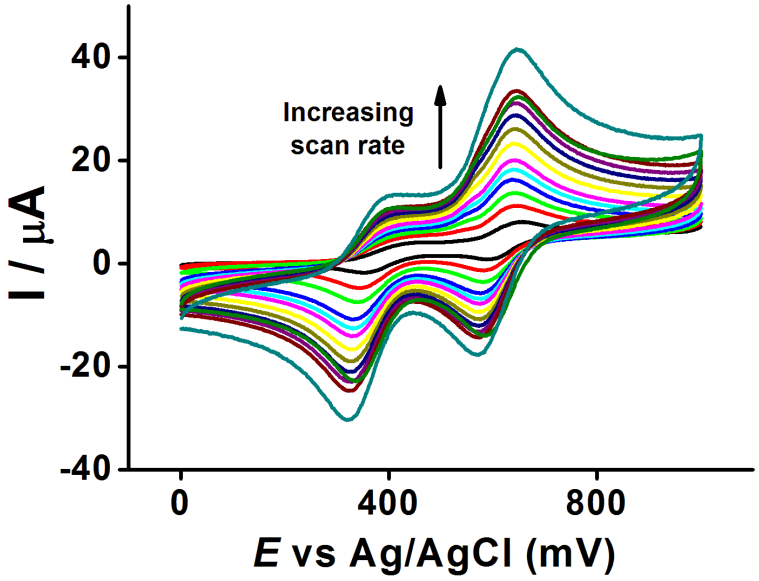

Fig. S8. Series of the second cycle CVs for **1**·4PF_6 taken at varying scan rates (50 to 1200 $mV \cdot s^{-1}$) (0.1 M $LiClO_4$ / 298 K / MeCN / versus Ag / AgCl).

6. Kinetic Studies by ^{1}H NMR Spectroscopy

For kinetic studies, an NMR tube containing CD_3COCD_3 was placed in a liquid nitrogen bath and a crystalline sample of the translational isomer **1R**·4PF_6 was added onto the CD_3COCD_3 solid. This tube was inserted into the probe of an NMR spectrometer (600 MHz), and cooled down to 190 K. After 1 h of equilibrating at 195 K, ^{1}H NMR spectra were recorded. The temperature was raised in 5 degree K increments every 20 minutes. No ^{1}H resonance integral change was observed until the probe temperature reached 220

K. At 220 K in CD_3COCD_3, **1R**·4PF_6 started to decay slowly to an equilibrium mixture of the translational isomers **1R**·4PF_6 and **1G**·4PF_6, and the rate was slow enough to be monitored (Fig. S9) by ^{1}H NMR spectroscopy.

The relaxation kinetics for the translational isomer **1R**·4PF_6 in CD_3COCD_3 were measured at 220 K using ^{1}H NMR spectroscopy. The molar percentage of translational isomer **1R**·4PF_6, over the total population of both the translational isomers **1R**·4PF_6 and **1G**·4PF_6, was determined from the integral for the ^{1}H resonances of the characteristic dioxynaphthalene unit. By plotting the **1R**·4PF_6 % against time, the half-life (τ) of this process was fitted using the first−order exponential decay formula:

$$\frac{N_A}{N_{tot}} = \frac{N_0}{N_{tot}} e^{-\frac{t}{\tau}} + \frac{N_\infty}{N_{tot}}$$

where N_A is the real time number of translational isomer **1R**·4PF_6 at time *t*, and N_{tot} is the total number of both translational isomers, N_∞ is the number of translational isomer **1R**·4PF_6 molecules when the solution reaches equilibrium (t = ∞),

$\Delta G^{\ddagger}$ was calculated from Eyring equation:

$$k = \frac{K_B T}{h} e^{\frac{-\Delta G^{\ddagger}}{RT}}$$

where *k* is the reaction rate constant, K_B is the Boltzman′s constant, *h* is the Planck′s constant, *T* is the absolute temperature and *R* is the gas constant.

Hence, the first order rate constant for the process **1R**·4PF_6→**1G**·4PF_6 (*k*) was calculated to be 7.31 (± 0.97) ×10^{-4} s^{-1}, indicating that the corresponding energy barrier for the circumrotation is 15.8 (± 0.05) kcal/mol at 220 K in CD_3COCD_3 (Fig. S10).

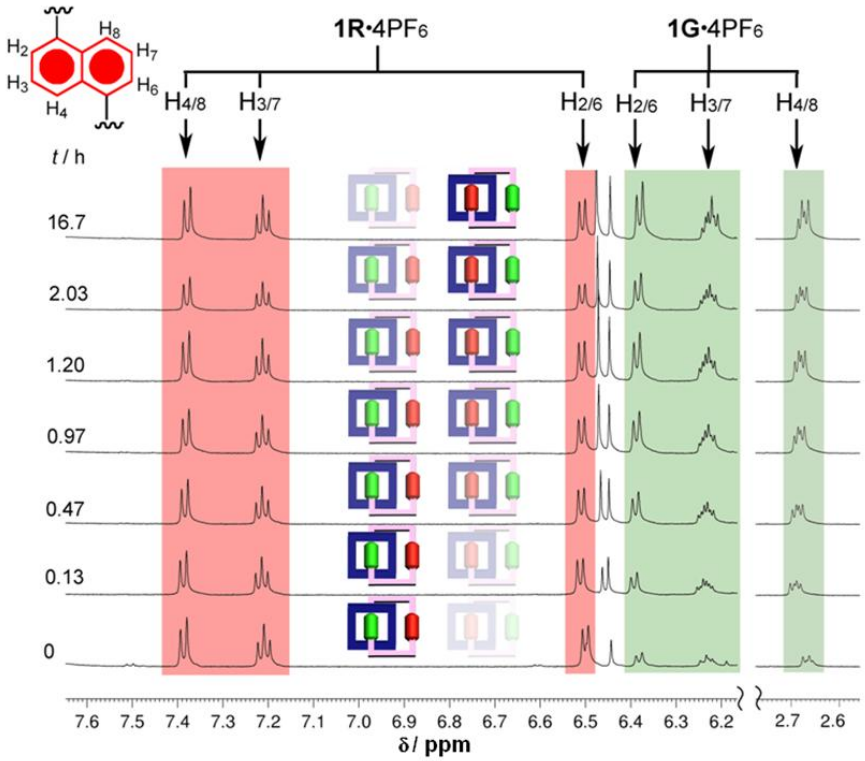

Fig. S9. Partial ^{1}H NMR spectra (600 MHz) of the translation isomer **1R**·4PF$_6$ recorded in CD_3COCD_3 at 220 K at different time (0 to 16.7 hours).

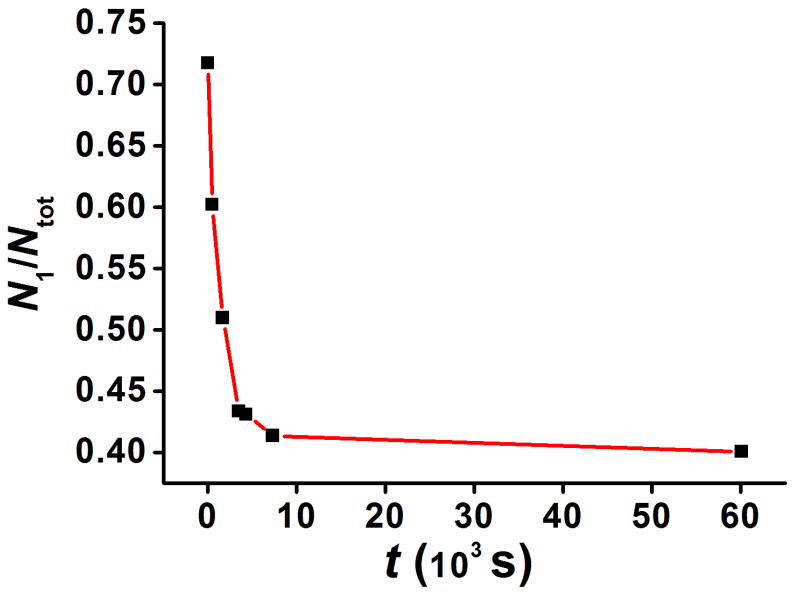

Fig. S10. Fitting the population ratios of the translational isomer **1R**·4PF$_6$ and the relaxation times to a first-order decay model.

9. X-Ray Analysis

Data Collection for 1R·4PF_6: A red tabular crystal of C_{76} H_{74} F_{24} N_8 O_8 P_4 S_6, having the approximate dimensions of 0.37 × 0.26 × 0.10 mm, was mounted using oil (Infineum V8512) on a glass fiber. All measurements were made on a CCD area detector with graphite monochromated MoK\α radiation. Cell constants and an orientation matrix for data collection corresponded to a triclinic cell with dimensions:

a = 13.7441(5) Å α = 78.1084(18)º

b = 14.6110(5) Å β = 84.8071(19)º

c = 22.4094(7) Å γ = 79.1998(18)º

V = 4319.3(3) Å^3

For Z = 2 and F.W. = 1999.67, the calculated density is 1.538 g·cm^{-3}. Based on a statistical analysis of intensity distribution, and the successful solution and refinement of the structure, the space group was determined to be $P\bar{1}$. The data was collected at a temperature of 100 K with a theta range for the data collection of 1.56 to 30.57º. Data were collected in 0.5º oscillations with 15 second exposures. The crystal-to-detector distance was 60.00 mm.

Data Reduction: Of the 30345 reflections which were collected, 12339 were unique (R_{int} = 0.0000). Data were collected using APEX2 V2.1-4 (6) detector and processed using SAINTPLUS from Bruker. The linear absorption coefficient, mu, for MoK\a radiation is 0.343 mm^{-1}. A multiscan absorption correction was applied, TWINABS V2008/1 (6). Minimum and maximum relative transmission factors were: 0.6556 to 1.0. The data were corrected for Lorentz and polarization effects.

Structure Solution and Refinement: The crystal under investigation was found to be non-merohedrally twinned. The orientation matrices for the two components were identified using the program CellNow (6), and the data were processed using both orientation matrices with SAINT, The exact twin matrix identified by the integration program was found to be: (1.000 – 0.330 – 0.065 / – 0.003 – 0.999 – 0.002 / 0.006 0.004 – 1.001). The second domain is rotated from first domain by 179.8° about the reciprocal lattice *a* axis. The absorption correction was carried out using TWINABS (6) to create an HKLF5 file which was used in all refinements; the structure was solved using direct methods. The twin fraction refined to a value of 0.397 (1).

The structure was solved by direct methods and expanded using Fourier techniques (7). The disordered fluorine and C18 atoms were refined with group anisotropic displacement parameters. The remaining non-hydrogen atoms were refined anisotropically. Hydrogen atoms were included in idealized positions but not refined. No hydrogen atoms were included for the two disordered MeCN molecules over four positions. The final cycle of full-matrix least-squares refinement (8) on F^2 was based on 30345 reflections and 1173 variable parameters and converged (largest parameter shift was 0.004 times its esd) with unweighted and weighted agreement factors of:

$$R_1 = \Sigma| \, |F_o|-|F_c| \, |/\Sigma|F_o| = 0.0838$$

$$wR_2 = \{\Sigma[w(F_o^2-F_c^2)^2]/\Sigma[w(F_o^2)^2]\}^{1/2} = 0.2023$$

The weighting scheme was calculated from the equation.

$$w=1/[\sigma^2(F_o^2)+(0.1162P)^2 + 0.0000P] \text{ where } P=(F_o^2+2F_c^2)/3$$

The standard deviation of an observation of unit weight (9) was 0.917. The weighting scheme was based on counting statistics and included a factor to downweight the intense reflections. Plots of $\Sigma w (|F_o| - |F_c|)^2$ versus $|F_o|$, reflection order in data collection, sin θ / λ and various classes of indices showed no unusual trends. The maximum and minimum peaks on the final difference Fourier map corresponded to +1.249 and –0.913 e·Å^3, respectively.

Neutral atom scattering factors were taken from Cromer and Waber (10). Anomalous dispersion effects were included in F_{calc} (11); the values for $\Delta F'$ and $\Delta F''$ were those of Creagh and McAuley (12). The values for the mass attenuation coefficients are those of Creagh and Hubbell (13). All calculations were performed using the Bruker SHELXTL3 crystallographic software package.

Data Collection for 1G·4PF_6**:** A green plate crystal of C_{82} H_{93} F_{24} N_{11} O_8 P_4 S_6, having approximate dimensions of 0.55 × 0.23 × 0.11 mm, was mounted using oil (Infineum V8512) on a glass fiber. All measurements were made on a CCD area detector with graphite monochromated MoKα radiation.

Cell constants and an orientation matrix for data collection corresponded to a triclinic cell with dimensions:

a = 13.6419(2) Å α = 98.7560(10)º

b = 13.9529(2) Å β = 104.8940(10)º

c = 26.1425(4) Å γ = 91.6640(10)º

V = 4740.72(12) Å^3

For Z = 2 and F.W. = 2132.91, the calculated density is 1.494 g·cm^{-3}. Based on a statistical analysis of intensity distribution, and the successful solution and refinement of the structure, the space group was determined to be $P\bar{1}$. The data was collected at a temperature of 100 K with a theta range for data collection of 1.48 to 24.71º. Data were collected in 0.5º oscillations with 15 second exposures. The crystal-to-detector distance was 60.00 mm.

Data Reduction: Of the 72375 reflections which were collected, 16126 were unique (R_{int} = 0.0665). Data were collected using APEX2 V2.1-4 (6) detector and processed using SAINTPLUS from Bruker. The linear absorption coefficient, mu, for MoKα radiation is 0.318 mm^{-1}. The data were corrected for Lorentz and polarization effects.

Structure Solution and Refinement: The structure was solved by direct methods and expanded using Fourier techniques (7). The non-hydrogen atoms were refined anisotropically. Hydrogen atoms were included but not refined. The final cycle of full-matrix least-squares refinemenet (8) on F^2 was based on 16126 reflections and 1223 variable parameters and converged (largest parameter shift was 0.033 times its esd) with unweighted and weighted agreement factors of:

$$R_1 = \Sigma| \, |F_o|-|F_c| \, |/\Sigma|F_o| = 0.0684$$

$$wR_2 = \{\Sigma[w(F_o^2-F_c^2)^2]/\Sigma[w(F_o^2)^2]\}^{1/2} = 0.1972$$

The weighting scheme was

$$w=1/[\sigma^2(F_o^2)+(0.1307P)^2 + 1.5439P] \text{ where } P=(F_o^2+2F_c^2)/3$$

The standard deviation of an observation of unit weight (9) was 1.062. The weighting scheme was based on counting statistics and included a factor to downweight the intense reflections. Plots of $\Sigma w (|F_o| - |F_c|)^2$ versus $|F_o|$, reflection order in data collection, $\sin\theta / \lambda$ and various classes of indices showed no unusual trends. The maximum and minimum peaks on the final difference Fourier map corresponded to +1.248 and –0.617 $e \cdot Å^3$, respectively.

Neutral atom scattering factors were taken from Cromer and Waber (10). Anomalous dispersion effects were included in F_{calc} (11); the values for $\Delta F'$ and $\Delta F''$ were those of Creagh and McAuley (12). The values for the mass attenuation coefficients are those of Creagh and Hubbell (13). All calculations were performed using the Bruker SHELXTL3 crystallographic software package.

Table S2. Crystal Data and Structure Refinement for **1R**·4PF_6

Empirical formula	C_{76} H_{74} F_{24} N_8 O_8 P_4 S_6
Formula weight	1999.67
Temperature	100 K
Wavelength	0.71073 Å
Crystal system, space group	Triclinic, $P\bar{1}$
Unit cell dimensions	a = 13.7441(5) Å, α =78.1084(18)º
	b = 14.6110(5) Å, β =84.8071(19)º
	c = 22.4094(7) Å, γ = 9.1998(18)º
Volume, V	4319.3(3) $Å^3$
Z, Calculated density	2, 1.538 $g \cdot cm^{-3}$
Absorption coefficient	0.343 mm^{-1}
F(000)	2044
Crystal size	0.37 × 0.26 × 0.10 mm
Theta range for data collection	1.56 to 30.57 º
Limiting indices	–19<=h<=19, –20<=k<=20, 0<=l<=32
Reflections collected / unique	30342 / 30345 [R_{int} = 0.0000]
Completeness to theta = 30.57	98.0 %
Absorption correction	Empirical, Twinabs (multi-scan)
Max. and min. transmission	0.9672 and 0.8848
Refinement method	Full-matrix least-squares on $F2$
Data / restraints / parameters	30345 / 0 / 1173
Goodness-of-fit on F^2	0.917
Final R indices [$I > 2\sigma(I)$]	R_1 = 0.0838, wR_2 = 0.2023
R indices (all data)	R_1 = 0.1934, wR_2 = 0.2424
Largest diff. peak and hole	+1.249 and –0.913 $e \cdot Å^{-3}$

Table S3. Crystal Data and Structure Refinement for **1G**·4PF_6

Empirical formula	C_{82} H_{93} F_{24} N_{11} O_8 P_4 S_6
Formula weight	2132.91
Temperature	100 K
Wavelength	0.71073 Å
Crystal system, space group	Triclinic, $P\,\bar{1}$
Unit cell dimensions	a = 13.6419(2)Å, α = 98.7560(10)º
	b = 13.9529(2)Å, β = 104.8940(10)º
	c = 26.1425(4)Å, γ= 91.6640(10)º
Volume, V	4740.72(12) $Å^3$
Z, Calculated density	2, 1.494 $g \cdot cm^{-3}$
Absorption coefficient	0.318 mm^{-1}
F(000)	2196
Crystal size	0.55 × 0.23 × 0.11 mm
Theta range for data collection	1.48 to 24.71º
Limiting indices	–16<=h<=16, –16<=k<=16, -30<=l<=30
Reflections collected / unique	72375 / 16126 [R_{int} = 0.0665]
Completeness to theta = 24.71	99.7 %
Absorption correction	Integration
Max. and min. transmission	0.9684 and 0.8988
Refinement method	Full-matrix least-squares on $F2$
Data / restraints / parameters	16126 / 0 / 1223
Goodness-of-fit on F^2	1.062
Final R indices [$I > 2\sigma(I)$]	R_1 = 0.0684, wR_2 = 0.1972
R indices (all data)	R_1 = 0.1044, wR_2 = 0.2206
Largest diff. peak and hole	+1.248 and –0.617 $e \cdot Å^{-3}$

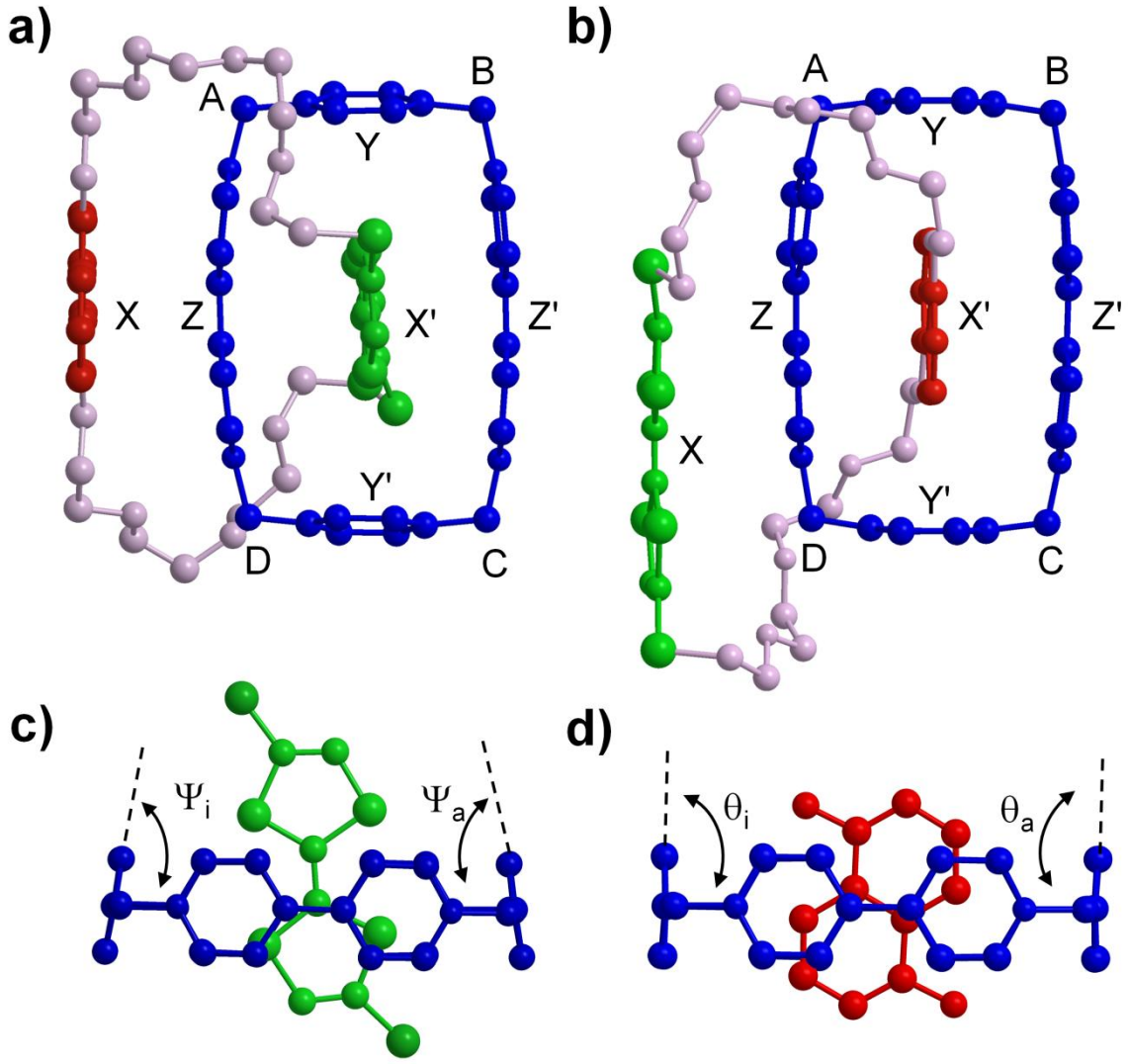

Fig. S11. A ball-and-stick representation of the solid-state crystal structures of **1R**$^{4+}$ (a, c) and **1G**$^{4+}$ (b, d), characterizing the molecular geometries (see Table S4).

Table S4. Distances (Å) and angles (^{o}) characterizing the molecular geometries of both translational isomers for **1**·4PF_6 [a].

Parameter	**1R**·4PF_6	**1G**·4PF_6
A [^{o}]	108.7	108.3
B [^{o}]	107.9	108.2
C [^{o}]	109.7	108.5
D[^{o}]	107.4	107.8
X···X' [Å]	6.95	7.55
Y···Y' [Å]	10.25	10.45
Z···Z' [Å]	6.94	6.61
X···Z [Å]	3.47	3.56
Z···X' [Å]	3.40	3.20
X'···Z' [Å]	3.33	3.28
Y···X' [Å]	3.50	3.42
Y'···X' [Å]	3.96	3.40
Ψi [^{o}]	81.30	———
Ψa [^{o}]	81.01	———
θi [^{o}]	———	89.1
θa [^{o}]	———	89.3
ϕZ [^{o}][b]	1.3	10.4
ϕZ' [^{o}][b]	4.8	-1.2
φZ [^{o}][c]	14.5	15.1
φZ' [^{o}][c]	14.4	10.2

[a] The distances and angles indicated in the table are illustrated in Fig. S11. [b] The twist angle ϕ is defined as the torsional angle about the central C–C bond of the bipyridinium unit. [c] The bowing angle φ is defined as the supplement of the angle subtended by the two N^{+}–CH_2 bonds attached to the bipyridinium ring system.

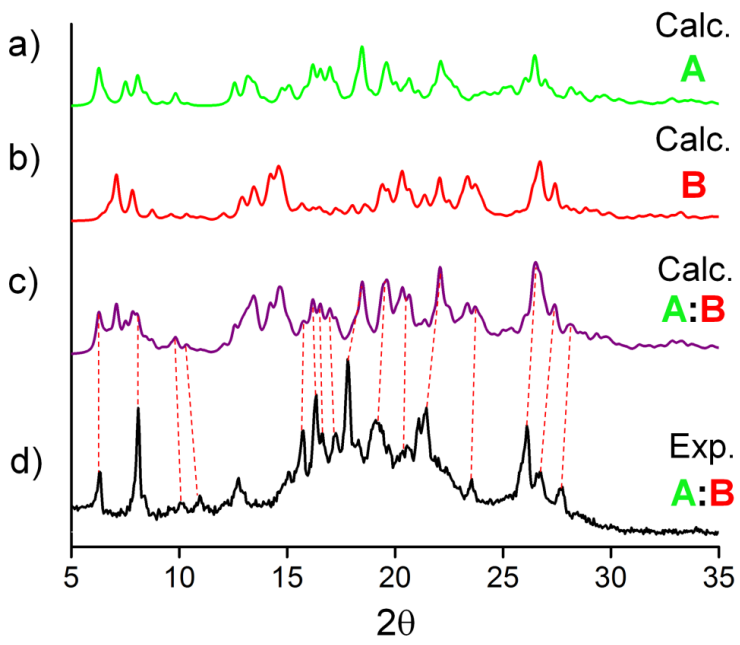

Fig. S12. A stack plot of X-ray powder diffraction (XRD) spectra drawing attention to the common peaks among the set —starting with the calculated spectra based on X-ray crystallographic data for **1R**·4PF_6 (a) and **1G**·4PF_6 (b) and their calculated 1:1 mixture (c) — which suggests the presence of both translational isomers in the equilibrated uncrystallized product **1**·4PF_6 as isolated from the reaction mixture, which was used to generate the experimental XRD spectrum (d). The calculated spectra was generated using Mercury crystallographic software at 1.5 Å with hydrogen atoms and a full width at half maximum (FWHM) value set at 0.3 2θ.

10. Computational Methods

All calculations were performed using density functional theory (DFT) as implemented in the Jaguar 7.6 software (14) Gas-phase geometry optimizations were performed at the M06/6-31G** level of theory. Natural bond orbital (15) analyses and molecular orbitals were obtained from the M06-HF/6-311++G** wavefunctions.

Front and Side Views of Molecular Orbitals

1R·4PF_6 Highest Occupied Molecular Orbital (HOMO)

E= −7.56 eV

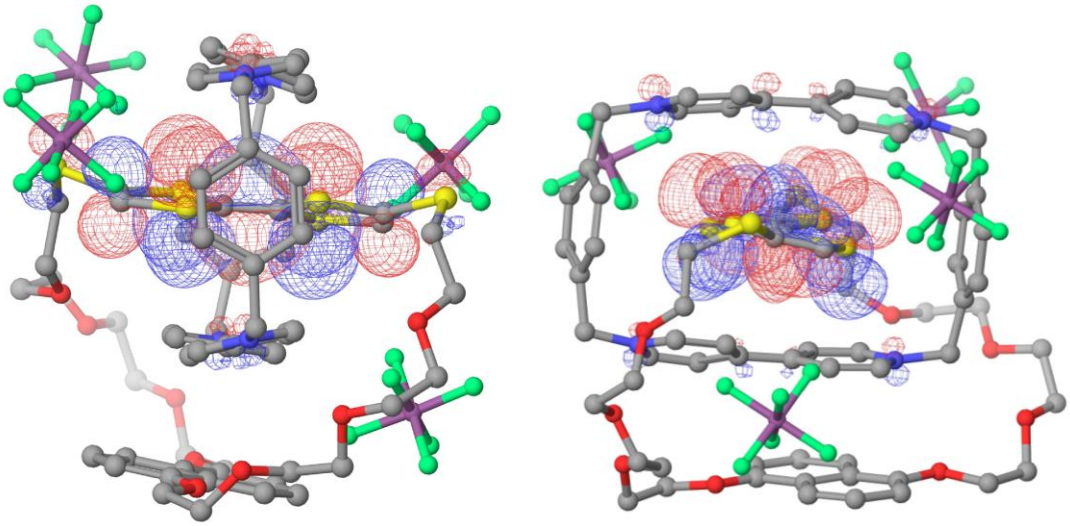

1R·4PF_6 HOMO−1

E= −8.81 eV

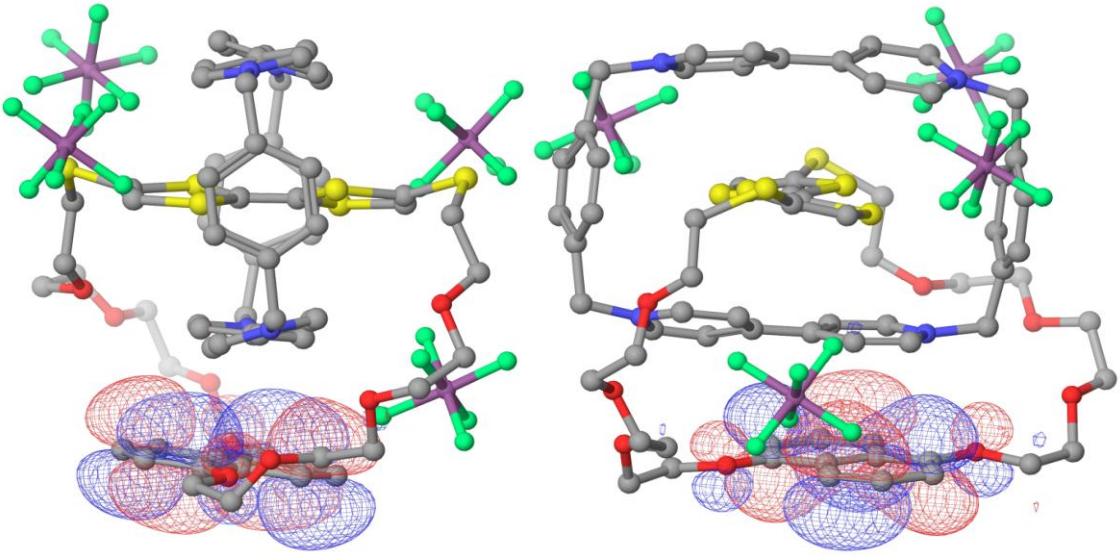

1R·4PF_6 HOMO−2

E=−9.04 eV

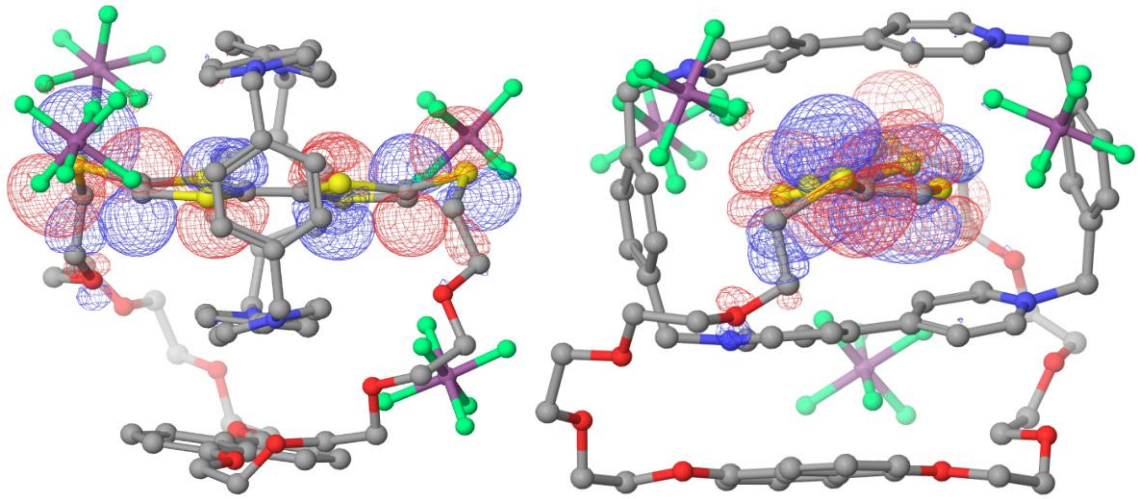

1R·4PF_6 Virtual Lowest Unoccupied Molecular Orbital (LUMO)

E= −1.79 eV (virtual)

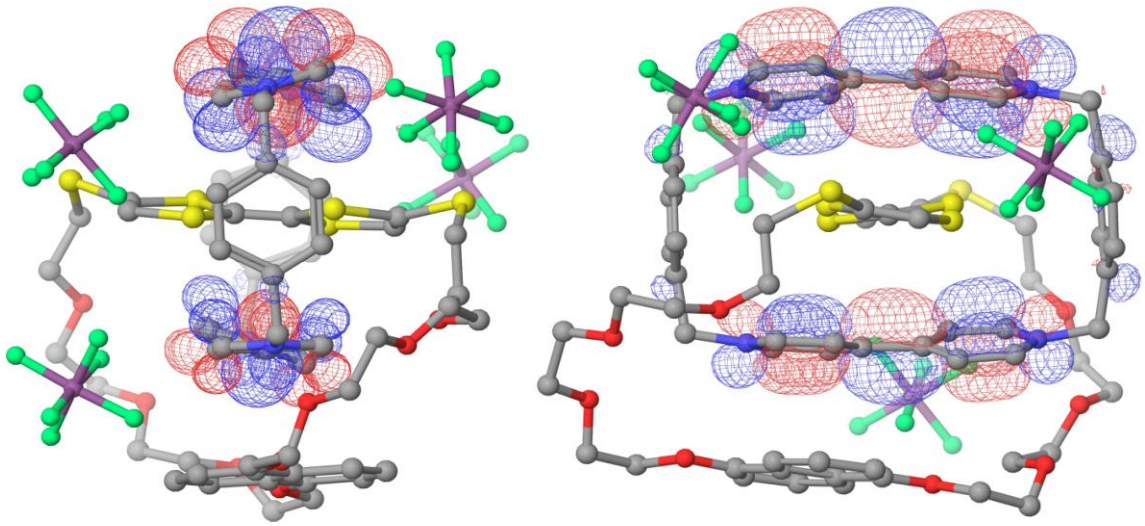

1G·4PF_6 Highest Occupied Molecular Orbital (HOMO)

E= −8.05 eV

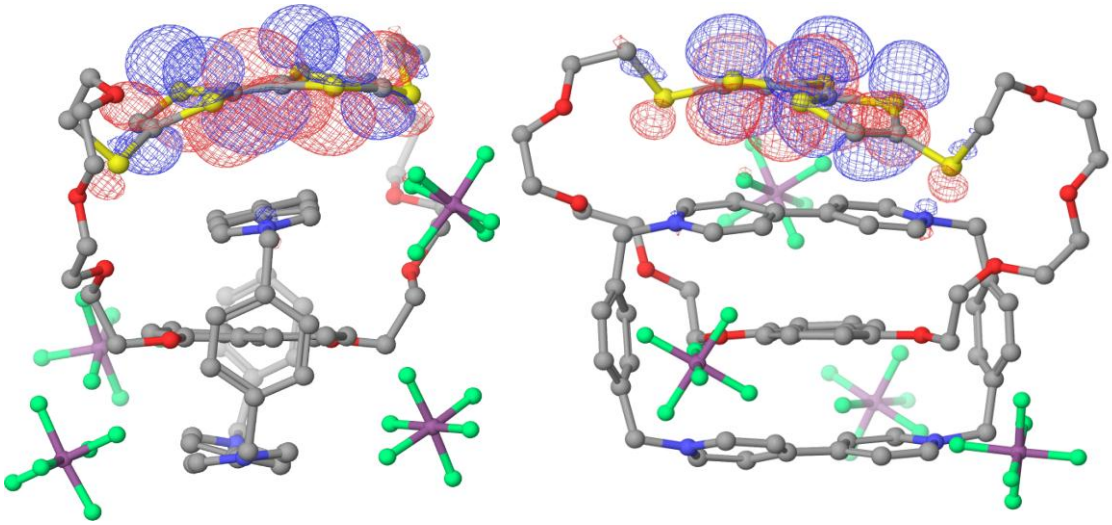

1G·4PF_6 HOMO−1

E= −8.49 eV

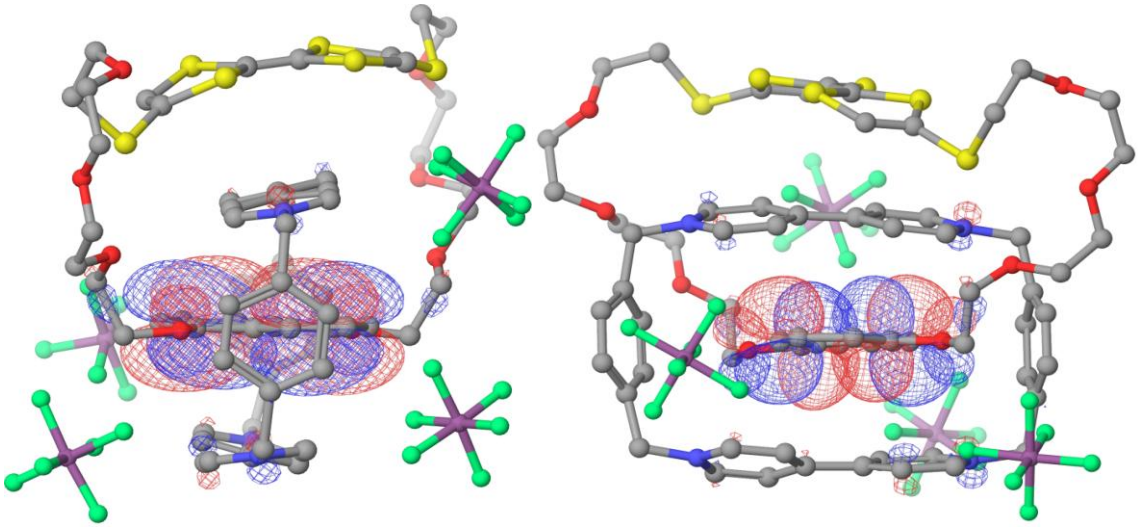

1G·4PF_6 HOMO−2

E= −9.53 eV

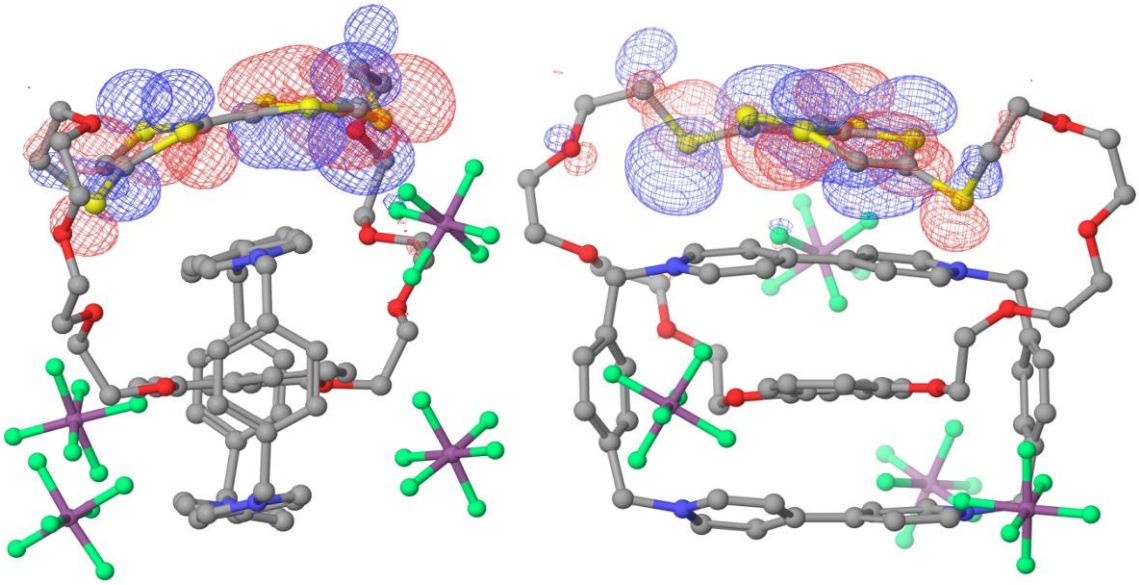

1G·4PF_6 Virtual Lowest Unnocupied Molecular Orbital (LUMO)

E= −1.92 eV (virtual)

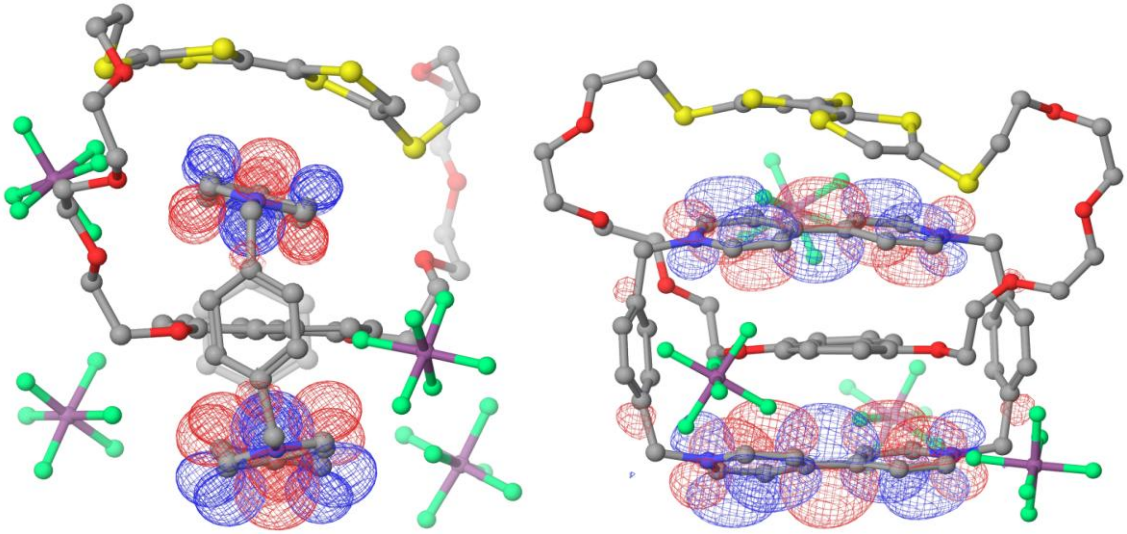

11. Reference

1 Jia CY, Zhang DQ, Xu W, Zhu DB (2001) A new approach to 4-alkylthio-1,3-dithiole-2-thione: An unusual reaction of a zinc complex of 1,3-dithole-2-thione-4,5-dithiolate. *Org Lett* 3:1941–1944.

2 Guo XF, *et al.* (2003) Donor-acceptor-donor triads incorporating tetrathiafulvalene and perylene diimide units: synthesis, electrochemical and spectroscopic studies. *Tetrahedron* 59:4843–4850.

3 Anelli PL, *et al.* (1992) [2]Rotaxanes and a [2]catenane made to order. *J Am Chem Soc* 114:193–218.

4 Asakawa, M, *et al.* (1996) Improved template-directed synthesis of cyclobis-(paraquat-*p*-phenylene). *J Org Chem* 61:9591–9595.

5 Ashton PR, *et al.* (1996) Bis[2]catenanes and a bis[2]rotaxane - Model compounds for polymers with mechanically interlocked components. *Chem Eur J* 2:31–44.

6 APEX2 V2.1-4 Bruker Analytical X-ray Instruments, Inc.: Madison, WI, 2007.

7 G. M. Sheldrick, SHELXTL Version 6.14; Bruker Analytical X-ray Instruments, Inc.: Madison, WI, 2003.

8 Full-Matrix Least-Squares refinement on F^2: $wR_2 = \{\Sigma[w(F_o^2-F_c^2)^2]/\Sigma[w(F_o^2)^2]\}^{1/2}$

9 GooF = S = $\{\Sigma[w(F_o^2-F_c^2)^2]/(n-p)\}^{1/2}$ n = number of reflections; p = total number of reflections refined.

10 Cromer DT, Waber JT (1974) in *International Tables for X-ray Crystallography* (The Kynoch Press, Birmingham, England) Vol. IV, Table 2.2 A .

11 Ibers JA, Hamilton, WC (1964) Dispersion corrections and crystal structure refinements. *Acta Cryst* 17: 781–782.

12 Creagh DC, Hubbell JH (1992) in *International Tables for Crystallography*, eds Wilson AJC (Kluwer Academic Publishers, Boston) Vol C, Table 4.2.4.3, pp 219–222.

13 Creagh DC, Hubbell JH (1992) in *International Tables for Crystallography*, eds Wilson AJC (Kluwer Academic Publishers, Boston) Vol C, Table 4.2.4.3, pp 200–206.

14 Jaguar, version 7.6, Schrödinger, LLC, New York, NY, 2009.

15 Glendening ED, *et al.* (2003) *NBO 5.0.* Theoretical Chemistry Institute, University of Wisconsin, Madison.